Chapter 5

Effect of Heat Treatment on Microstructural Properties of AA7075 and AA7020 Alloys[1]

Uğur Büyük[2]

Emin Çadırlı[3]

Hasan Kaya[4]

Erkan Üstün[5]

Abstract

AA7075 and AA7020 alloys were prepared using a vacuum melting furnace and a casting furnace. Microstructural properties of the alloy samples were examined in both as-cast and heat-treated conditions. In order to investigate the effect of heat treatment, various designed AA7075 and AA7020 samples were homogenized in two steps (300 °C/12h+475 °C/12h) and then aged under different regimes. The effects of heat treatment on the microstructures were studied using optical microscopy (OM), scanning electron microscopy (SEM)/energy-dispersive X-ray (EDX) elemental analysis, transmission electron microscopy (TEM), and X-ray diffraction (XRD) analysis. The microstructural properties of both alloy systems (AA7075 and AA7020) were compared both within themselves and with each other, depending on how they were exposed to heat treatment. The analysis of EDX and XRD patterns reveal that the aged AA7075 and AA7020 alloys contain α-Al matrix phase, $MgZn_2$ and Al_2CuMg intermetallics, with the $MgZn_2$ IMC phase being the only one detected in the aged AA7020 alloy sample,

1 This work was supported by the Erciyes University Scientific Research Project Unit under contract No's: FBA-2021-10981. The authors are grateful for the financial support.

2 Prof. Dr., Erciyes University, Faculty of Education, Department of Science Education, Kayseri, Turkey, buyuk@erciyes.edu.tr, ORCID: 0000-0002-6830-8349

3 Prof. Dr., Niğde Ömer Halisdemir University, Faculty of Arts and Sciences, Department of Physics, Niğde, Turkey, ecadirli@gmail.com, ORCID: 0000-0002-8085-9733

4 Prof. Dr., Erciyes University, Faculty of Education, Department of Science Education, Kayseri, Turkey, hasankaya@erciyes.edu.tr, ORCID: 0000-0003-3529-9762

5 Dr., Niğde Ömer Halisdemir University, Institute of Science, Niğde, Turkey, erkanustun_07@hotmail.com, ORCID: 0000-0002-7745-396X

https://doi.org/10.58830/ozgur.pub60.c264

which is evident from the TEM micrographs showing polyhedral shaped Al_2CuMg particles about 30-50 nm in size and spherical shaped $MgZn_2$ particles about 10-30 nm in size dispersed in the eutectic phase and at the grain boundaries.

INTRODUCTION

The remarkable properties of aluminum have made it an essential material in numerous areas of engineering. With its low density and strength-to-weight ratio, it is widely used in construction and in the manufacture of structural parts of vehicles such as automobiles, engines and aircrafts. Furthermore, its recyclability and energy-efficiency render it a sustainable material. To maximize the potential of aluminum, research is being conducted on its alloys, heat treatment and forming technologies. Of all heat-treatable aluminum alloys, 7xxx series is the most significant. Age hardening has been found to dramatically enhance its properties (Hatch, 1984; Rometsch, Zhang & Knight, 2014). Thus, this alloy is often preferred in applications requiring high strength.

Aging of the alloy brings about better mechanical properties due to the hindrance of dislocation motion caused by the precipitates formed from the heat treatment. This procedure is made up of three stages: solution, quenching and aging. During the solution step, the material is heated to a temperature high enough to create a single-phase solid-solution with abundant alloying elements. The quenching process follows, in which the material is cooled rapidly to maintain the supersaturated microstructure at room temperature. The last step is aging, in which the alloy is stored at a particular temperature for a certain period of time, resulting in the formation of a secondary phase in the structure. In order for the aging heat treatment to take place, one or more alloying elements in the alloy must be completely or highly soluble in the matrix (Mouritz, 2012). The aging ability of 7xxx alloys is due to the high dissolution of the Zn and Mg elements they contain (Chinh *et al.,* 2014). With the sudden decrease in temperature during quenching, the solubility of the matrix decreases. Zn and Mg dissolved in the matrix are pushed out of the lattice and aggregate to form a secondary phase. Since these secondary phases make the dislocation movement difficult during deformation, an increase in the strength of the material occurs. If this situation is expressed in more detail, Zn and Mg atoms dissolved in the supersaturated solid solution (η) after quenching due to the effect of aging temperature come together and form regions compatible with the matrix crystal lattice. These regions are called Guinier–Preston (GP regions) regions. In the subsequent aging stages, with the increase of atoms clustered

in the GP regions, the second phase, which is meta-stable with the matrix crystal lattice and expressed as η', is formed. In the following aging stages, the η' phase precipitates as a stable η'-$MgZn_2$ secondary phase, which is incompatible with the matrix crystal lattice (Berg *et al.,* 2001). The usual precipitation sequence of the 7xxx alloys can be summarized as follows (Berg *et al.*, 2001; Ogura, Hirosawa & Sato, 2004; Polmear, 1958; Ringer and Hono, 2000; Dellah *et al.*, 2013; Shaa and Cerezo, 2004; Starink and Wang, 2003; S. Liu *et al.*, 2015; Wang, Yin & Sun, 2007; Liu *et al.*, 2010; Orovcik *et al.*, 2016; Lapin, Marecek & Kursa, 2006; Chen *et al.*, 2009; Wu *et al.*, 2010);

supersaturated solid solution (α–Al) → GP zones →metastable η′→stable η ($MgZn_2$).

Two distinct GPZs, GPI and GPII, exist in aged Al-Zn-Mg alloys, with their structures differing from each other. GPI zones are coherent with the aluminum matrix and are formed across an ample temperature range, from room temperature to 140-150°C, regardless of the quenching temperature (Shaa and Cerezo, 2004). GPII zones are Zn-rich layers and can be created upon quenching from a temperature higher than 450°C, followed by aging at temperatures over 70°C (Berg *et al.,* 2001; Shaa and Cerezo, 2004). In most cases, GPI or both GPI and GPII zones act as precursors to the metastable η′ phase. This metastable hardening precipitate is formed directly from the solid solution at temperatures higher than 100-120°C (Berg *et al.,* 2001). The main hardening precipitate η′ is a metastable hexagonal phase that is semi-coherent with the aluminum matrix. During the later stages of precipitation, the η′ phase undergoes a transformation into its stable η form. The equilibrium phase, η, can be generated right from the solid solution. As per the peak aged condition (T6), the predominant precipitate phases are a mixture of η′ and stable η (Starink and Wang, 2003). Subsequently, this paper aimed to evaluate and compare the microstructural and ductility properties of AA7075 (Al-5.5Zn-2.5Mg-1.5Cu wt.%) and AA7020 (Al-4.5Zn-1.2Mg-0.15Cr-0.15Zr wt.%) alloys after being subjected to a succession of heat treatments, including homogenization and aging. This particular research has not evaluated the effects of heat treatment on the microstructure of the two alloys in a comparative manner. Therefore, the microstructures and ductility of the alloys were inspected to discern the effects of the heat treatment.

EXPERIMENTAL PROCEDURES

Preparation of the AA7075 and AA7020 cast alloys

High purity (99.99%) Al, Zn, Mg, Cu and minor metals (Cr, Zr) were utilized to manufacture the AA7075 and AA7020 cast alloys (all compositions are indicated in wt.% unless otherwise stated). The Al was put in a graphite receptacle (L:170 mm, OD: 40 mm, ID:30 mm) and melted in a vacuum furnace. After the Al had been completely dissolved, the requisite amount of Zn was laid beneath the surface of the molten Al. Then the Al-Zn amalgam was stirred three times with a five-minute interval and the necessary amount of Mg was encased with pure thin Al foil and within a graphite cage that had numerous perforations (Fig. 1a) and placed beneath the surface of the liquid Al-Zn alloy to prevent Mg burning on the surface of the melt. Finally, copper and other trace metals (chromium and zirconium) necessary for the specific alloy were added to the crucible and heated until melted. To ensure homogeneity of the alloy, the molten metal was melted again in a vacuum furnace and the billet was then inverted. After stirring and allowing sufficient time for homogenization, the alloy was poured through a funnel into a graphite crucible connected to alumina molds (180 mm in length, 9 mm OD, 6 mm ID) that were placed in the casting furnace (Fig. 1b and c). The furnace was set to temperatures of approximately 50 ^{o}C and 100 ^{o}C above the melting point of the alloy in the upper and lower heaters, respectively. Each sample was stirred with a fine alumina rod and then solidified from the bottom up using a water-cooled stainless-steel reservoir in order to obtain a completely mixed and directionally solidified homogeneous sample.

The samples of two alloys, namely AA7075 and AA7020, were produced in the necessary quantities for microstructure analysis in this research. The average cooling rates observed in the directionally solidified samples varied from 8 to 2 K/s, depending on the position relative to the reservoir. As part of the sample preparation process, experiments were repeated until the desired number of suitable samples were obtained. Subsequently, the 10 mm upper and lower regions of the sample, which may contain casting defects, were removed and excluded from the mechanical testing. The remaining parts of the samples were then prepared for microstructure examination, mechanical evaluation, and quantitative analysis. The samples were then subjected to a homogenization process consisting of two stages; 300°C/12h followed by 475°C/12h. Afterwards, they were quenched in water at room temperature. In order to compare the alloy samples with those in as-cast form, two of the samples were preserved in a freezer at

-18°C, thus avoiding natural aging of the alloy at room temperature. The other 10 samples were split into five subgroups, with one group left as only homogenized, while the remaining four were exposed to various aging regimes. Four distinct subgroups were exposed to a T6 artificial aging process under various conditions, identified as regime 1-regime 4. To ensure reliable data, two specimens were allocated to each subgroup. A Protherm PLF 110/45 model muffle furnace was utilized to perform the solution heat treatment (T6). This process initially involved keeping the samples at 300°C for 12 hours, followed by 475°C for 12 hours and then quenching in water at room temperature for supersaturated solid solution α–Al. Subsequently, an artificial aging process was done with four regimes: regime 1 (120°C/24h), regime 2 (150°C/24h), regime 3 (120°C/12h +150°C/12h) and regime 4 (150°C/12h +180°C/12h). A summary of the heat treatment conditions for both solution treatment and aging process is presented in Table 1.

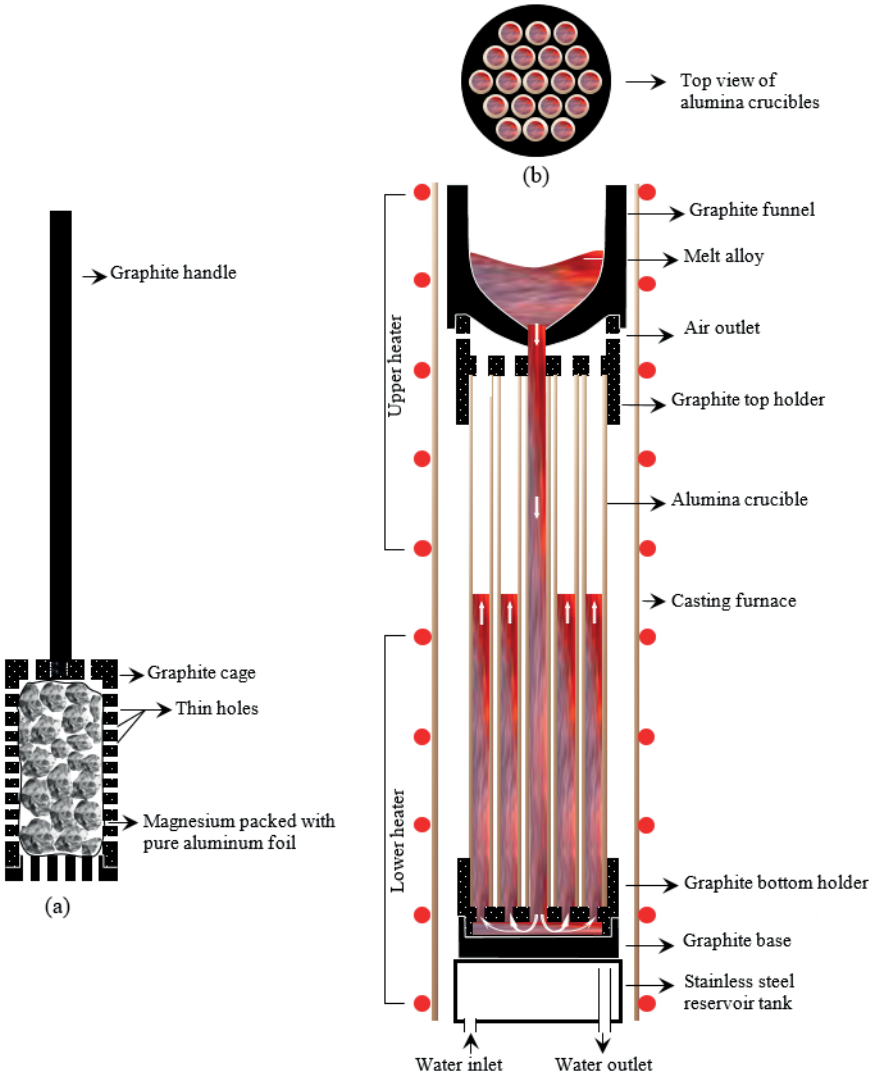

Figure 1. (a) Graphite cage (b) Top view of alumina crucibles (c) Crucibles in the casting furnace

Table 1. Heat treatment processes of the AA7075 and AA7020 alloys

Name of sample	Process	Status
WHT	Without heat treatment	As-cast
OH	Only Homogenization	300 °C/12h+475 °C/12h (two-step)
Regime 1	H+artificial aging	300 °C/12h+475 °C/12h→120°C/24h (one-step)
Regime 2	H+artificial aging	300 °C/12h+475 °C/12h→150°C/24h (one-step)
Regime 3	H+artificial aging	300 °C/12h+475 °C/12h→120 °C/12h+150 °C/12h (two-step)
Regime 4	H+artificial aging	300 °C/12h+475 °C/12h→150 °C/12h+180 °C/12h (two-step)

Microstructure characterization and identification of phases

Sections from each sample were fashioned with cold molding material (e.g. epoxy resin) before undergoing the process of mechanical grinding, polishing and etching with Keller's reagent (2 mL HF, 3 mL HCl, 5 mL HNO_3 and 190 mL water) for 10 seconds. Subsequently, the microstructures of all the samples were examined using an inverted Nikon Eclipse MA 100 optical microscope as well as a Zeiss-Gemini 500 FESEM coupled with an energy dispersive X-ray (EDX) spectrometer and a computer-controlled image system. This enabled the composition of the matrix and intermetallic compound (IMC) phases in the specimens to be determined with the help of EDX analysis at 20 keV using X-ray lines. Additionally, X-ray diffraction (XRD) analysis was employed to verify the accuracy of the data obtained from EDX analysis. XRD measurements were carried out with a diffractometer (Rigaku Ultima IV) utilizing Cu-Kα radiation (k=1.5405 A°) at an accelerating voltage of 40 kV. Subsequently, the diffracted beam was scanned in steps incrementing by 0.01° across a 2θ range of 30-90°.

The morphology of aged AA7075 and AA7020 samples were investigated using transmission electron microscopy (TEM) (JEOL SEM-100SX), operating at a voltage of 300 kV and a double-tilt stage. To this end, TEM foils were made from the aged samples. Subsequently, 3 mm discs were cut from the foils and then thinned to perforation by using twin-jet electropolishing with a 10 wt.% perchloric acid in methanol solution, at

a voltage of 20Vdc. The outcomes of the EDX/mapping, XRD and TEM analyses, along with comments, are provided in the following section.

RESULTS AND DISCUSSION

Heat treatment

As-cast specimens usually feature dendritic microstructures composed of both α-Al solid solution and non-equilibrium phases that settle on grain boundaries and the interdendritic regions during solidification. During this process, there is an uneven distribution of α-Al solid solution and intermetallics, which can cause composition segregation. Moreover, variations of cooling rates, temperatures, and inclusions of impurities, metallic or non-metallic components can lead to inhomogeneous microstructures and properties (Wang *et al.,* 2014). To improve the as-cast microstructures, heat treatments such as homogenization and aging, as well as solutions of non-equilibrium phases, can be applied (Wang *et al.,* 2014). If heat treatments are employed, it should be noted that the temperature should not exceed the lowest melting point of the phase in the sample (Nayan *et al.,* 2009). This will cause dendritic segregation to decline gradually and unstable phases to transform into stable ones. In conclusion, heat treatments can eliminate inhomogeneities of alloys, thus improving the performance and quality of the products.

Microstructure characterization

The mechanical characteristics of the material are predominantly determined by the microstructures; therefore, OM, SEM and TEM were used to assess the composition of the phases, and EDX/elemental mapping and XRD were used to identify their chemical composition. The corresponding OM and SEM microstructures of the WHT and HT samples of both the AA7075 and AA7020 alloys are demonstrated in Figures 2-3.

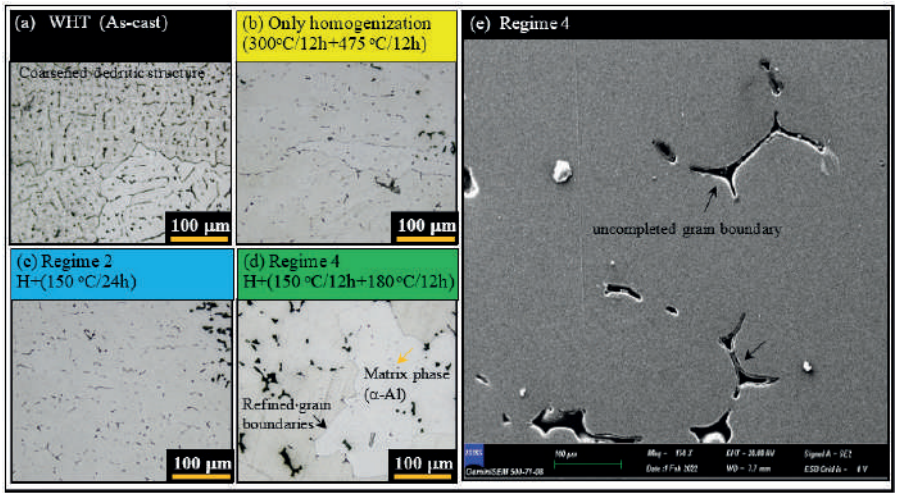

Figure 2. Typical optical and SEM micrographs for the AA7075 alloy (a) As-cast (WHT) (b) Only homogenization (c) Regime 2 (d) Regime 4 (e) Regime 4 (SEM image)

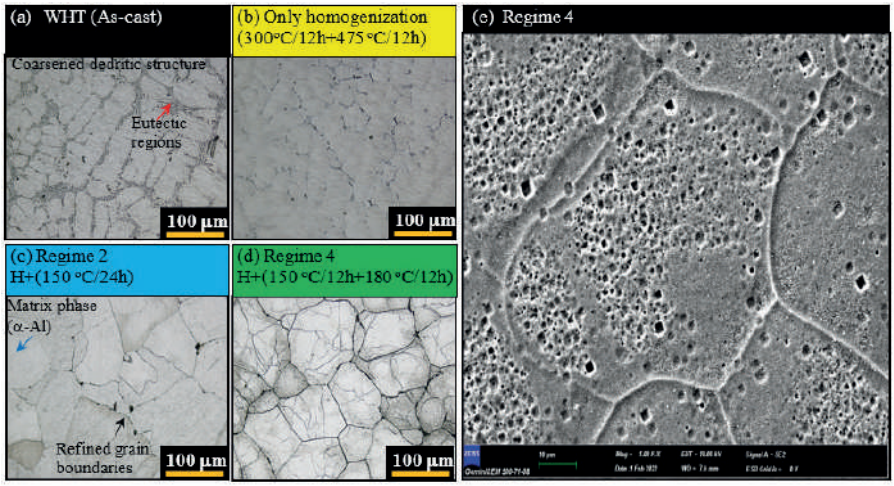

Figure 3. Typical optical and SEM micrographs for the AA7020 alloy (a) As-cast (WHT) (b) Only homogenization (c) Regime 2 (d) Regime 4 (e) Regime 4 (SEM image)

As can be seen from Figs.(2a-3a), dendritic structures in the casting sample are seen for both alloys. Although the dendritic structure is coarsened in both structures, eutectic structures are occasionally observed between the coarsened dendrite arms, especially for the AA7020 alloy (Fig. 3a). As can be seen from Figure 2b-3b, for both alloys, dendritic structures disappeared and grain boundaries became coarser in solution treated samples (only homogenization). Figures 2(c-d)-3(c-d) show the structures in the one-step

and two-step aging process applied after homogenization. While incomplete grain boundaries were observed in AA7075 alloys that had undergone these aging processes (regimes 2 and 4), more distinct grain boundaries and completed hexagonal cells were observed in AA7020 alloys. This is more clearly seen in the SEM images given in Figures 2e-3e.

As can be seen in Fig. 4, chemical results of the heat treated alloys (regime 4) are given in the EDX spectrum and elemental mapping analysis. The microstructures observed in the samples analyzed for both alloys (region 4) mainly consist of the main phase and the secondary phases containing intermetallic compounds. As can be seen from the table values given in the EDX spectrum (Fig. 4a), the composition values for the aged AA7075 sample (regime 4) were determined as 91.90 Al, 4.66 Zn, 2.34 Mg and 1.10 Cu (wt.%). As seen from the EDX spectrum given in Figure 4b, composition values of 93.50 Al, 3.83 Zn, 1.61Mg, 0.67 Zr and 0.39Cr (wt.%) were determined for the aged AA7020 sample (regime 4). These composition values determined for both alloy samples aged in the same regime (regime 4) are very close to the nominal compositions. However, for the AA7020 alloy, the Cr and Zr values were slightly higher than the nominal values. As well as the presence of α-Al matrix phase, for the AA7075 and AA7020 samples that aged at regime 4, $MgZn_2$ and Al_2CuMg intermetallics were observed in the grain boundary and small eutectic regions. While both $MgZn_2$ and Al_2CuMg IMC phases were detected in the aged AA7075 alloy sample (regime 4), only the $MgZn_2$ IMC phase was detected in the aged AA7020 alloy sample (regime 4).

Similar results were found by Deng et al. (Deng *et al.*, 2012) and Gonzales et al. (Gonzales *et al.*, 2003). In the mapping analysis given in the spectrum on the right part of the same figure (Fig. 4), the distribution of each Al, Zn, Mg, Cu, Cr and Zr elements within the measurement regions was obtained with different colors. The constituent phases in the aged AA7075 and AA7020 alloy samples were determined with XRD analysis. The XRD patterns of the aged alloys are shown in Fig. 5.

As indicated, the presence of α-Al (matrix-phase), $MgZn_2$ (η-phase) and Al_2CuMg (S-phase) is confirmed due to the high number of peaks corresponding to these matrix phase and IMC phases, respectively. Both EDX analysis (Fig. 4) and XRD pattern (Fig. 5) strongly indicate that there are three phases (α-Al, $MgZn_2$ and Al_2CuMg) for the aged AA7075 alloy (regime 4) and two phases (α-Al, $MgZn_2$) for the aged AA7020 alloy (regime 4).

The TEM micrograph in Figure 6 of aged AA7075 and AA7020 samples (regime 4) after being homogenized (300°C/12h+475°C/12h) clearly shows that Al_2CuMg (S-phase) and $MgZn_2$ (η-phase) precipitates (IMCs) have formed. In the micrograph, these particles were identified as polyhedral shaped and spherical in shape, respectively. Additionally, the precipitates showed different shapes, including the bigger, dark polyhedral Al_2CuMg particles and the smaller, open spherical $MgZn_2$ particles. The size of Al2CuMg particles was determined to be 30-50 nm, while the size of $MgZn_2$ particles ranged from 10-30 nm and were dispersed throughout the eutectic phase and at the grain boundaries.

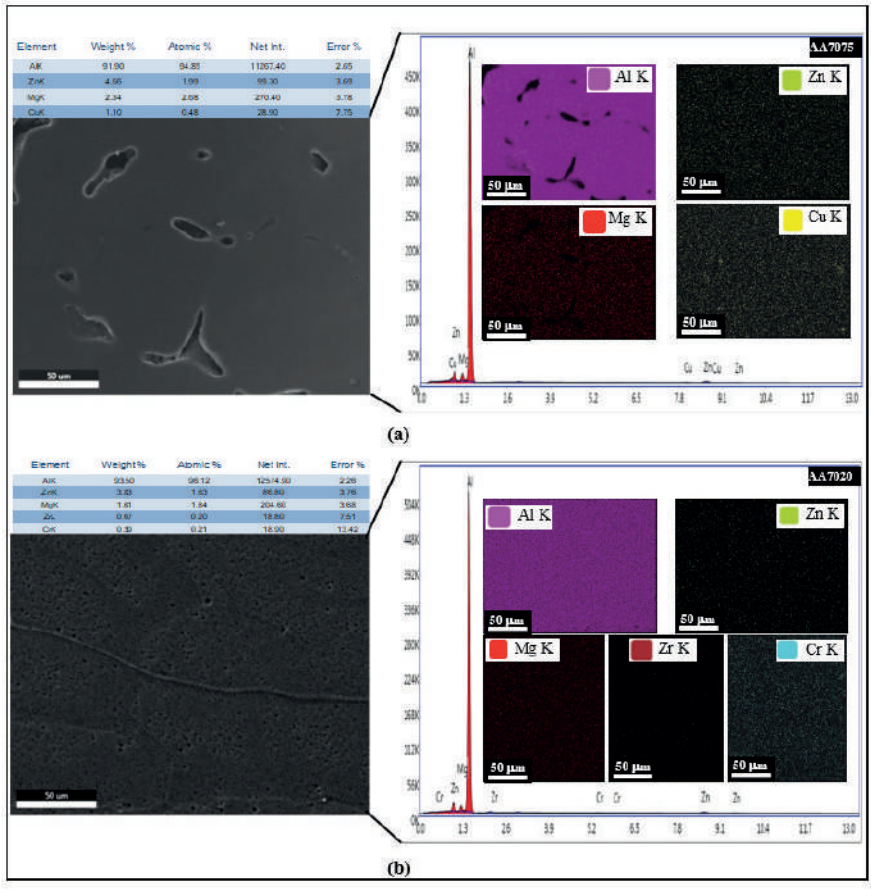

Figure 4. EDX spectrum and elemental mapping analysis for studied alloys (a) AA7075 alloy (Regime 4) (b) AA7020 alloy (Regime 4)

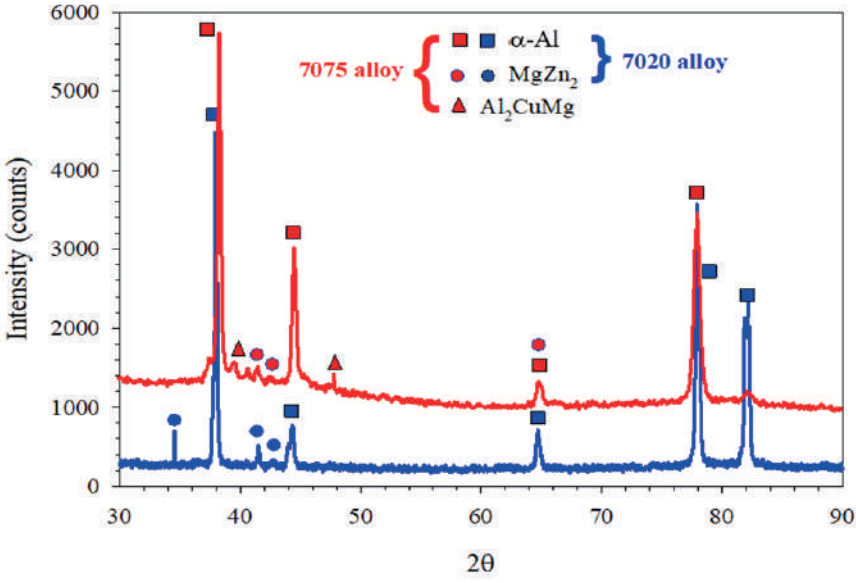

Figure 5. XRD patterns obtained from the aged samples (Regime 4) of the AA7075 and AA7020 alloys

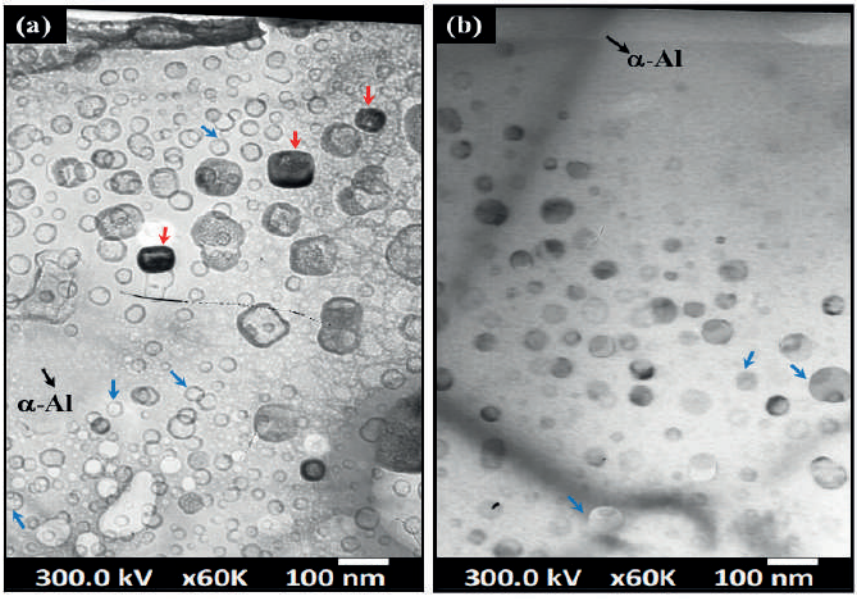

Figure 6. (a) TEM micrograph of $MgZn_2$ (blue arrow) and Al_2CuMg (red arrow) precipitates in the AA7075 sample aged with the aging regime 4 (150 °C/12h +180 °C/12h) after the homogenization (12 h at 300 °C+12 h at 475 °C) (b) TEM micrograph of $MgZn_2$ (blue arrow) precipitates in the AA7020 sample aged with the aging regime 4 (150 °C/12h +180 °C/12h) after the homogenization (12 h at 300 °C+12 h at 475 °C). The α-Al phase, which is the matrix phase for both alloys, is shown with a white arrow.

CONCLUSION

AA7075 and AA7020 alloys were produced using the vacuum furnace and the casting furnace. Microstructure properties of as-cast and heat-treated samples were investigated. The key findings are given as follows:

i. The microstructures of AA7075 and AA7020 alloys in their as-cast state include both dendritic α-Al solid solution and non-equilibrium phases that tend to form along grain boundaries and in the interdendritic spaces during solidification.

ii. Although the dendritic structure is coarsened in both structures, eutectic structures are occasionally observed between the coarsened dendrite arms, and more distinct grain boundaries and completed hexagonal cells are observed in AA7020 alloys after aging processes.

iii. The analysis of EDX and XRD patterns show that the aged AA7075 alloy has three phases (α-Al, $MgZn_2$ and Al_2CuMg) while the aged AA7020 alloy has two phases (α-Al, $MgZn_2$).

iv. The presence of α-Al matrix phase, $MgZn_2$ and Al_2CuMg intermetallics in the grain boundary and small eutectic regions were detected in the aged AA7075 and AA7020 samples, with the $MgZn_2$ IMC phase being the only one detected in the aged AA7020 alloy sample.

v. The TEM micrograph showed that Al_2CuMg and $MgZn_2$ precipitates have formed in the aged AA7075 and AA7020 samples, with polyhedral shaped Al_2CuMg particles about 30-50 nm in size and spherical shaped $MgZn_2$ particles about 10-30 nm in size dispersed in the eutectic phase and at the grain boundaries.

ACKNOWLEDGMENTS

This work was supported by the Erciyes University Scientific Research Project Unit under contract No's: FBA-2021-10981. The authors are grateful for the financial support.

REFERENCES

A. P. Mouritz, Introduction to Aerospace Materials. Cambridge, England: Woodhead Publishing Ltd. (2012). (ISBN 978-1-84569-532-3)

C. Gonzales, O. Alvarez, J. Genesca, J.A. Juarez-Islas, Solidification of chill-cast Al-Zn-Mg alloys to be used as sacrificial anodes, Metall. Mater. Trans. A 34 (2003) 2991–2997. https://doi.org/10.1007/s11661-003-0198-6

G. Sha, A. Cerezo, Early-stage precipitation in Al–Zn–Mg–Cu alloy (7050), Acta Mater. 52 (2004) 4503–4516. https://doi.org/10.1016/j.actamat.2004.06.025

H. Wang, J. Xu, Y. Kang, M. Tang, Z. Zhang, Study on inhomogeneous characteristics and optimize homogenization treatment parameter for large size DC ingots of Al–Zn–Mg–Cu alloys. J. Alloys Compd. 585 (2014) 19–24. https://doi.org/10.1016/j.jallcom.2013.09.139

I.J. Polmear, The upper temperature limit of stability of GP zones in ternary aluminium–zinc–magnesium alloys, J. Inst. Metals 87 (1958–1959) 24–25.

J. Buha, R.N. Lumley, A.G. Crosky, Secondary ageing in an aluminium alloy 7050, Mater. Sci. Eng. A 492 (2008) 1–10. https://doi.org/10.1016/j.msea.2008.02.039

J. Chen, L. Zhen, S. Yang, W. Shao, S. Dai, Investigation of precipitation behavior and related hardening in AA 7055 aluminum alloy, Mater. Sci. Eng. A 500 (2009) 34–42. https://doi.org/10.1016/j.msea.2008.09.065

J. E. Hatch, Aluminum: properties and physical metallurgy. Metals Park, Ohio: American Society for Metals, 1984. ISBN: 978-0-87170-176-3

J. Lapin, J. Marecek, M. Kursa, Effect of heat treatments on the microstructure and mechanical properties of directionally solidified multiphase intermetallic Ni-Al-Cr-Ta-Mo-Zr alloy, Kovove Mater. 44 (2006) 1–11.

L. Orovcik, M. Nosko, J. Kovacik, T. Dvorak, M. Stepanek, F. Simancik, Effects of chemical composition on the pore structure and heat treatment on the deformation of PM aluminium foams 6061 and 7075, Kovove Mater. 54 2016 463–470. DOI: 10.4149/km 2016 6 463

L.K. Berg, J. Gjønnes, V. Hansen, X.Z. Li, M. Knutson-Wedel, D. Schryvers, L.R. Wallenberg, GP-zones in Al–Zn–Mg alloys and their role in artificial aging. Acta materialia, 49(17) (2001) 3443–3451. https://doi.org/10.1016/S1359-6454(01)00251-8

L.M. Wu, M. Seyring, M. Rettenmayr, W.H. Wang, Characterization of precipitate evolution in an artificially aged Al–Zn–Mg–Sc–Zr alloy, Mater. Sci. Eng. A 527 (2010) 1068–1073. https://doi.org/10.1016/j.msea.2009.09.023

M. Dellah, M. Bournane, Kh.A. Ragab, Y.Sadaoui, A.F. Sirenko, Early decomposition of supersaturated solid solutions of Al–Zn–Mg casting

alloys, Mater. Des. 50 (2013) 606–612. https://doi.org/10.1016/j.matdes.2013.02.078

M.J. Starink, S.C. Wang, A model for the yield strength of overaged Al–Zn–Mg–Cu alloys, Acta Mater. 51 (2003) 5131–5150. https://doi.org/10.1016/S1359-6454(03)00363-X

N. Nayan, S. Y. S. N. Murty, Gotvind, M. C. Mittal, P. P. Sinha, Optimization of homogenizing mode for aluminum alloy AAAA7075 using calorimetric and microstructural studies, Met. Sci. Heat Treat. 51 (2009) 330–337. https://doi.org/10.1007/s11041-009-9178-9

N.Q. Chinh, J. Lendvai, D.H. Ping, K. Hono, The effect of Cu on mechanical and precipitation properties of Al–Zn–Mg alloys. J. Alloys Compd. 378(1–2) (2004) 52–60. https://doi.org/10.1016/j.jallcom.2003.11.175

P. A., Rometsch, Y. Zhang, S. Knight, Heat treatment of 7xxx series aluminium alloys - Some recent developments. Transactions of Nonferrous Metals Society of China (English Edition), 24 (7), (2014) 2003–2017. https://doi.org/10.1016/S1003-6326(14)63306-9

S. Liu, C. Li, S. Han, Y. Deng, X. Zhang, Effect of natural aging on quench-induced inhomogeneity of microstructure and hardness in high strength 7055 aluminum alloy, J. Alloys Compd. 625 (2015) 34–43. https://doi.org/10.1016/j.jallcom.2014.10.195

S. Liu, J. You, X. Zhang, Y. Deng, Y. Yuan, Influence of cooling rate after homogenization on the flow behavior of aluminum alloy 7050 under hot compression, Mater. Sci. Eng. A 527 (2010) 1200–1205. https://doi.org/10.1016/j.msea.2009.10.055

S. P. Ringer, K. Hono, Microstructural evolution and age hardening in aluminium alloys: atom probe field-ion microscopy and transmission electron microscopy studies, Mater. Charact. 44 (2000) 101–131. https://doi.org/10.1016/S1044-5803(99)00051-0

T. Ogura, S. Hirosawa, T. Sato, Quantitative characterization of precipitate free zones in Al–Zn–Mg(–Ag) alloys by microchemical analysis and nanoindentation measurement, Sci. Technol. Adv. Mater. 5 (2004) 491–496. https://doi.org/10.1016/j.stam.2004.02.007

T. Wang, Z.M. Yin, Q. Sun, Effect of homogenization treatment on microstructure and hot workability of high strength 7B04 aluminium alloy, Trans. Nonferrous Met. Soc. China 17 (2007) 335–339. https://doi.org/10.1016/S1003-6326(07)60094-6

Y. Deng, Z.Yin, K.Zhao, J.Duan, Z.He, Effects of Sc and Zr microalloying additions on the microstructure and mechanical properties of new Al–Zn–Mg alloys, J.Alloy.Compd.530 (2012)71–80. https://doi.org/10.1016/j.jallcom.2012.03.108